Nuclear Inst. and Methods in Physics Research, A 927 (2019) 125–132

Contents lists available at ScienceDirect

Nuclear Inst. and Methods in Physics Research, A

journal homepage: www.elsevier.com/locate/nima

Validation of the energy-loss response of α particles in iC_4H_{10} with ACTARSim

P. Konczykowski [a], B. Fernández-Dominguez [a,*], H. Alvarez-Pol [a], M. Caamaño [a], G.F. Grinyer [b,c], A.T. Laffoley [c,1], B. Mauss [c], J. Pancin [c], D. Pérez-Loureiro [c], T. Roger [c]

[a] Dpt. de Física de Partículas Univ. of Santiago de Compostela and IGFAE, E-15758, Santiago de Compostela, Spain
[b] Department of Physics, University of Regina, Regina, SK S4S 0A2, Canada
[c] GANIL (CEA/DSM-CNRS/IN2P3), BP 5027, 14076 Caen Cedex, France

ARTICLE INFO

Keywords:
TPC
Active target
Simulation
ACTARSim
Energy loss profile

ABSTRACT

ACTARSim is a framework based on Geant4 and ROOT to simulate the response of active targets for nuclear physics experiments with radioactive beams. In this paper, we present the performance of the simulations for the energy-loss profile, total energy, range and angular resolution of the reconstructed track. Validation of the ACTARSim software against experimental data was performed in iC_4H_{10} with a mixed alpha source using the ACTAR TPC demonstrator. The results show a good agreement with the simulations indicating the validity of the models used in ACTARSim for α-particles in iC_4H_{10}.

1. Introduction

Gas-filled time projection chambers and active-targets have been used in particle and nuclear physics experiments for almost thirty years. Since then, the field of Time Projection Chambers (TPCs) for use as active targets in nuclear physics studies is steadily growing worldwide.

First experiments with radioactive beams combined with active targets have addressed very interesting physics cases covering a wide range of topics. These include the study of matter distribution of exotic nuclei with proton elastic scattering using IKAR [1,2] at GSI, the two-proton radioactivity observed with the CENBG TPC [3,4], properties of exotic nuclei such as the halo structure of ^{11}Li [5,6] and the first measurement of the unbound ^{7}H system [7] with MAYA [8] at GANIL.

In particle physics, a similar technique will be applied to electron–proton elastic scattering at the MAMI accelerator (Mainz University) [9] and to muon–proton elastic scattering at SPS accelerator at CERN to measure the proton radius with unprecedent precision.

This type of detector exploits the sensitive gas volume inside the TPC to act also as a target where the reaction takes place. The operation principle is based upon the ionization of the atoms of the gas volume by the charged particles along its trajectory and the drift of the released electrons under an electric field towards a sensitive x–y anode. By measuring the induced charge and the drift time, the tracks of the charged particles within the gas can be deduced.

Active target detectors offer unique tracking abilities and provide means of reconstructing the interaction point in three dimensions (3D). These systems present several advantages over standard detection equipment: the ability to act as a relatively thick target without loss of resolution, a large efficiency and a low-energy threshold. These advantages make them particularly suitable devices to modern nuclear physics experiments. In particular, experiments with radioactive beams of limited intensity performed in inverse kinematics are often combined with active targets to boost the luminosity of the reaction.

However, several factors such as poor energy resolution and a reduced dynamic range restricted the performance of the first-generation devices. Recent technological advances have overcome the limitations of the first-generation detectors and improved the capabilities in terms of multitracking, customized gains and thresholds and smaller pixel sizes. Several active targets are therefore being developed across the world for studies with low intensity radioactive beams. Examples of ongoing projects include ACTAR TPC [10] at GANIL, AT-TPC [11] at NSCL, the SπRIT TPC at RIKEN [12] and the ACTAF project at GSI [13].

In order to plan, analyze, and interpret the resulting experimental data measured with active targets, reliable simulations are needed. The ACTARSim [14] code was developed to simulate the active target response and to assess the feasibility of certain key experiments. The code is based on the Geant4 [15] Monte Carlo toolkit to simulate the passage of particles through the detector and a set of functions based on the ROOT analysis framework [16] to reproduce the electron drift and amplification on the pad plane. The electron drift parameters used in the simulations are calculated by the MAGBOLTZ code [17]. Formerly used to optimize the geometry of the ACTAR TPC [10] project, this simulation tool can easily be adapted for other gas-filled detection

* Corresponding author.
E-mail address: beatriz.fernandez.dominguez@usc.es (B. Fernández-Dominguez).
[1] Present Address: Department of Physics, University of Guelph, Guelph, ON N1G 2W1, Canada.

https://doi.org/10.1016/j.nima.2019.02.013
Received 29 August 2018; Received in revised form 4 February 2019; Accepted 5 February 2019
Available online 10 February 2019

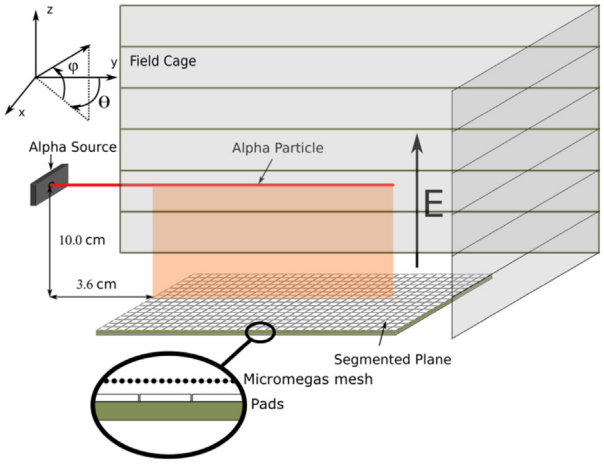

Fig. 1. Schematic view of the experimental setup.

systems. The framework allows the user to define new geometries and to incorporate auxiliary detectors. The simulations include the physics performance and a detailed detector response. From the simulated results, appropriate algorithms and analysis tools are developed to reconstruct key observables. Experimental data can thus be analyzed in exactly the same way as the simulated results. For the general simulation purposes of ACTARSim, the drift and diffusion of the electrons are based on statistical models, instead of microscopic descriptions such as, for instance, GARFIELD/GARFIELD++ [18,19].

Key observables of the foreseen experiments with active targets are the drift time, and the longitudinal and transverse profile of the energy-loss of charged particles within the gas; they are related to the kinematical quantities of the involved particles such as angle and range (see Section 2). Simulations can then model the deposited energy in the active gas and reconstruction procedures can be applied to determine the trajectory of a given charged particle with high quality. An accurate simulation is therefore crucial to improve the resolution and identify the reaction channel. Validation of the ACTARSim toolkit for the reconstructed energy-loss profiles was done by benchmarking the simulations against experimental measurements obtained with a triple-alpha source using the ACTAR TPC demonstrator [10]. The ACTAR TPC [10] project based at GANIL, funded by the European Research Council (ERC) in 2014, is one of the European efforts for the construction of an upgraded active target for nuclear physics studies. The demonstrator is a prototype built and commissioned to optimize the detector parameters at the design stage used to determine the final geometry.

The present article focuses on the validation of energy-loss deposition and track reconstruction of charged-particles obtained with the ACTARSim software. This paper first describes the key observables and discusses the required resolutions in Section 2. A brief description of the experimental setup is shown in Section 3. Section 4 presents a general overview of the processes included in the simulations and the track reconstruction algorithms used to obtain the energy-loss profiles with ACTARSim. Experimental results are compared to simulations in Section 5.

2. Experimental observables

The ACTAR TPC project will address a rich research program covering many modern, relevant topics in nuclear physics [10] with nuclear structure studies and exotic decays establishing the major guidelines for the detector design and requirements.

In nuclear physics experiments one aims at deducing some physical quantities such as: excitation energy, angular correlations, cross sections or excitation functions. In the case of active targets without a solenoidal magnet, these can be obtained from the measurement of the total energy and/or the angle of the outgoing particles that stop within the gas volume. The measured resolutions, with active targets without magnet, for the total energy and the horizontal and vertical angles are typically of the order of $\Delta E/E < 3.5\%$ and of $\Delta\theta$ (FWHM) and $\Delta\phi$ (FWHM) $< 1°$ [3,11,20,21]. Furthermore, a clean identification of the outgoing particles can be used to reduce any other source of background such as interactions with other atoms from the gas molecule of which would be of no interest for the experiment.

With active targets, the kinetic properties of the charged particles have to be reconstructed from the drift time and the charge collected by each pad. For instance, the particle trajectory is estimated from the horizontal and vertical angles, and the energy of the outgoing particles can be calculated from either the range of the particle in the gas (R) or from the total charge deposited in the pads (Q_{tot}). The total charge and the range are determined by the energy loss profile of the particle along the track. The total charge is determined from the integration of the profile while the range is determined from the position where the energy loss is equal to half the maximum value after the Bragg peak. Therefore, precise simulations of the energy loss profile with an accurate reproduction of the shape are crucial to compare the Bragg curve to the one obtained experimentally. The energy loss profile contains the information of the energy and the range of a given ion. An excellent track resolution is required to attain the desired vertex resolution ($\Delta(X_{vertex},Y_{vertex})$ (FWHM) < 1 mm). By consequence, the quality of the simulations should be better than the experimental resolution.

In this paper, we have assessed the performance of the reconstruction techniques used in the ACTARSim software. In some cases, estimations of the uncertainties associated to the fitting track algorithms and reconstruction procedure are also evaluated.

3. Experimental setup

The ACTAR TPC demonstrator is a scaled-down version of ACTAR TPC detector with a rectangular geometry [10]. The dimensions of the gas volume are 240×190 mm^2 in the horizontal plane and 210 mm in height. Inside the chamber, the active volume is defined by a surface of 128×64 mm^2 in the horizontal plane and by a vertical height of 170 mm. The wire field cage is placed 5 mm from the edge of the active volume to ensure the homogeneity of the electric field within the active area. The detector anode consists of square pads of 2 mm sides arranged in a 64×32 configuration with 2048 total pixels. The amplification system uses the bulk-micromegas technology with a 220 μm amplification gap [22,23]. The micromegas concept divides the detector in two-regions. The first region, also called drift region, is where the primary ionization and charge drift take place under a moderate electric field. In the second region or amplification stage, the strong electric field produces the multiplication of the charges and the signals are read-out in the pad plane. Signals from the 2048-pads are treated and recorded using the GET [24] electronics which is comprised of four ASIC chips (AGET) coupled to a 12-bit Analog–Digital Convertor (ADC) in an AsAd card (ASIC and ADC). Each AGET contains 64 physical channels and 4 Fixed Pattern Noise (FPN) channels to record the intrinsic noise. The signals are continuously sampled and stored in a circular memory of 512-samples for each channel. The concentration of the flux of the 8 AsAd boards is achieved using two Concentration Boards (CoBo). A Multiplicity Trigger and Time module (MuTant) is used to distribute 100 MHz clock signals to synchronize the whole system.

A triple alpha source of ^{239}Pu, ^{241}Am and ^{244}Cm with main decay energies of 5.15, 5.48 and 5.8 MeV, respectively, was placed 10 cm above the micromesh and 36 mm before the horizontal pad plane, or active area (Fig. 1). The source was located outside the field cage with no collimation. However, a region of 5×5 pads, chosen with the theoretical range of the alpha particles, was used as a trigger for the measurement. This region is located at approximately 100 mm away from the source. The multiplicity level trigger, defined as L1 in reference [24] was set to

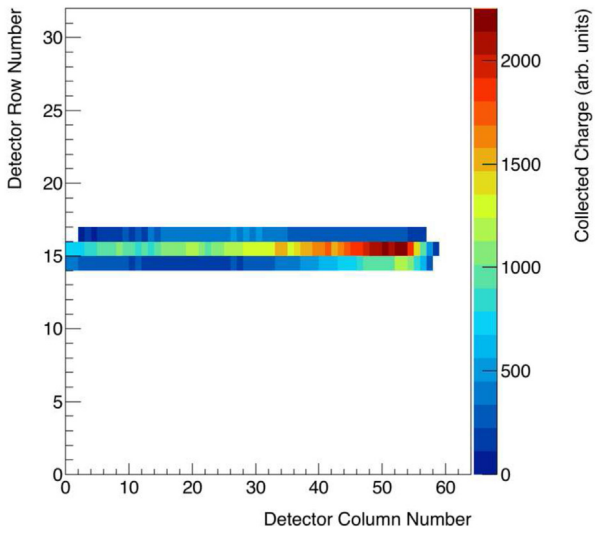

Fig. 2. Pad charge visualization of an alpha track. Color code corresponds to the charge measured in the ADC.

5 pads hit. This selection on the central pads allowed us to accept only tracks with small horizontal angles, $|\theta|$ <4° and vertical angles $|\phi|$ <15° (see the inset in Fig. 1 for the coordinate reference system).

A gas-handling system ensured a continuous and adjustable flow and pressure inside the chamber. The gas used for the experiment was iC_4H_{10} at 105.6 mbar. The pressure was chosen such that the alpha particles would stop inside the active region while covering most of the pad plane when emitted horizontally (see Fig. 2). During the run, the temperature was monitored by a temperature sensor (T = 25(1) °C). No significant temperature variations were observed.

Electrons produced by the gas ionization along the trajectory of a charged particle drift towards the anode. The gas volume is divided in two regions, the first one with a low field zone, where the initial ionization takes place, and a second one, corresponding to the small gap between the micromegas and the pads, with a high field, where the electrons from the drift are amplified. For this test, the electric fields in the drift and amplification region were set to 125 V/cm and about 16 kV/cm, respectively. In the amplification region, the electrons undergo a strong electric field generating an avalanche multiplication that induces a charge in the pads. The individual charges are collected on each pad and processed in the front-end GET electronics cards. The signals were sampled at a frequency of 25 MHz and recorded in a 12-bit ADC with a peaking time of 1014 ns and a dynamic range of 240 fC. Each channel has an individual trigger corresponding to a certain value above the noise level (around 2000 electrons).

Each pad signal carries two sets of information which will be used for analysis: the amplitude of the signal, which is proportional to the collected charge, and the time. The absolute drift time is obtained from the arrival time with respect to a start signal which is given by the ancillary detectors, usually silicon detectors placed at forward angles. It is important to note that for the present study, no auxiliary detectors were used. The drift time is calculated as the time difference between the time reference and the rest of pads. The time reference is defined as the first arrived pad in the 5 × 5 pad zone used for the trigger.

4. Actarsim software and reconstruction method

ACTARSim is a code based on Geant4 and ROOT used for the simulation of active targets and time projection chambers for nuclear physics experiments [14]. The Geant4 simulation toolkit is used for the set-up description, primary-event generator and particle tracking while a ROOT based program is used for the electron drift and amplification configuring the pad response.

4.1. Particle tracking and signal digitization

The first phase of the simulation implements the tracking of the particles inside the detector using the Geant4 Monte Carlo toolkit. In this first part, the full detector configuration, including the geometry of the detector, type of gas, temperature and pressure, is defined. In addition, an event generator of a specific reaction channel of interest is also incorporated at this stage. For the particle transportation and physical interactions processes the electromagnetic (EM) standard package with the Option 3 (Opt 3) parameters-list was used. Alpha particles from the particle generator of the simulation interact with the user-defined material (in this case iC_4H_{10} at 105.6 mbar and a temperature of 25 °C) along their trajectories by losing energy or producing secondary particles. Interaction points, corresponding either to a defined portion of energy loss or to the production of delta electrons above a given threshold energy (E_{cut} = 1 keV), contain all the primary particle information (energy loss, position and particle momentum) and are stored as steps.

During the second phase of the simulation, also called digitization, the steps are processed in a set of functions defined using ROOT to reproduce the detector response: number of electrons produced during the ionization process, their drift and diffusion to the anode micromesh by the electric field, and the amplification in the micromegas section. We consider that all the energy deposited in the gas is converted into electron–ion pairs. The mean number of primary ionization electrons (N_p) produced is given by the ratio between the deposited energy and the pair production energy (the energy loss required to produce an electron–ion pair); in isobutane $W_{iC_4H_{10}} = 23$ eV [25]. In the detector, the primary electrons drift under an applied uniform electric field. In the simulation the interaction points are transported over the full vertical distance, h, to the pad plane with a constant drift velocity v_{drift}. The point-like cloud spreads over this drift distance. Electron drift parameters such as the drift velocity v_{drift} (36.43 × mm/μs) and the transverse and longitudinal diffusion coefficients D_T (24.94 × 10^{-2} mm^2/μs), D_L (20.62 × 10^{-2} mm^2/μs) are taken from MAGBOLTZ [17] as a function of the electric field. The incoming position of the electrons on the amplification plane is randomized according to a Gaussian distribution with a standard deviation equal to:

$$\sigma_T = \sqrt{2 D_T h / v_{drift}} \tag{1}$$

where h is the vertical height of the step center, defined as the average position between the initial and final positions of a given step. The resulting value of the transversal dispersion is σ_T= 1.7 mm, which is of the order of the pad size. In the amplification region, the primary electrons acquire enough energy to produce secondary ionization electrons (N_s) developing an electron avalanche over the full distance from the micromesh to the anode pad plane inside the micromegas. A multiplicative factor, chosen by the user in order to match the data, is applied to describe the gain of the amplification region. In order to account for gain fluctuations, a Polya distribution [26] was applied to the electrons to parametrize the effective micromegas amplification. The output structure of the detector response simulation is equivalent to the experimental data stream. Therefore a common analysis program is used for both simulations and real data.

4.2. Track reconstruction

The trajectories of the particles inside the chamber are reconstructed from the (x, y, z) coordinates along their track. The (x, y) coordinates are obtained from the position of the pad plane. The third dimension is extracted from the drift time assuming a constant drift velocity, v_{drift}. The reconstruction is performed using different algorithms providing information on: the horizontal and vertical angles (θ, ϕ) and the induced charge, Q, which is used for both: total energy measurement and energy loss profile to determine the range of particles inside the gas volume.

For the angle determination, the reconstructed trajectory is obtained from the digitized signals and the individual times recorded in each pad.

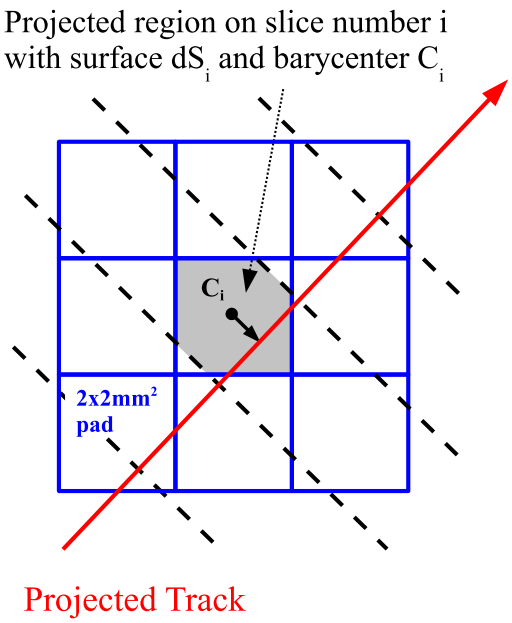

Fig. 3. Scheme of the weighted pad projection method. The dashed lines represent the size of the slices perpendicular to the particle trajectory. The shadow area, dS_i, displays the region outlined by a slice delimited by the dashed lines and a given pad with index i. The barycenter C_i corresponds to the geometric center of the dS_i region.

The orthogonal distance to a straight line, weighted by the charge in each pad is minimized in three dimensions. The 3D track-fitting provides the best choice of parameters for each trajectory.

In order to obtain the energy profile and the total energy, the 3D-fitted track is projected onto the pad plane. The pad plane is subdivided in a series of slices perpendicular to the track direction in 2D (see Fig. 3). The slice size was set to 2 mm, corresponding to the pad size, so as to optimize the statistical fluctuations arising from the choice of a smaller slice size and the loss in resolution by selecting a larger one. Each slice contains several regions that are outlined by the slice surface perpendicular to the trajectory of the particle in 2D and the individual pads (see shadow region in Fig. 3). The charge in each slice is defined, Q^{slice}, is defined as the sum of the collected charge per pad Q_i^{pad}, weighted by the surface ratio span by the slice dS_i (Fig. 3),

$$Q^{slice} = \sum_{i=1}^{N} \frac{dS_i}{S^{pad}} Q_i^{pad} \tag{2}$$

where S^{pad} is equal to 2×2 mm^2. This method provides a direct profile of the particle energy loss in the gas along its trajectory on an event-by-event basis. In order to compare them with the experimental results, many simulated profiles have been added together so as to reduce the uncertainty resulting from the simulations. The longitudinal profile of each event is affected by energy straggling, thus the curves need to be aligned with respect to the "End Point", which corresponds to the last bin with significant charge. The average profile fully characterizes the energy loss of a given particle in a given gas.

In order to validate the performance of the ACTARSim reconstruction methods, simulated data were compared to the data used as input in the simulations.

Concerning the reconstruction procedure, we have compared the reconstructed angles (θ_{rec}, ϕ_{rec}) obtained using the 3D-fit, to the angles of the particle within the gas derived from the interaction points simulated by Geant4 (θ_{sim}, ϕ_{sim}) and to the initial ones (θ_0, ϕ_0) used to generate the event. For this test we simulated 5.8 MeV alphas in 105.6 mbar of iC_4H_{10}. The alpha track length is typically of the order of 60 pads (see Fig. 2).

The top panels of Figs. 4 (a) and (b) show the angular uncertainty of the reconstruction procedure. The standard deviations of the $\theta_{sim} - \theta_{rec}$ and $\phi_{sim} - \phi_{rec}$ distributions give information on the precision of the algorithms used in the reconstruction technique. Since the straggling is included in both variables *sim* and *rec*, the width of the difference measures the effect of the reconstruction method, as the drift is considered negligible. For the horizontal angle, θ, the reconstruction is observed to be remarkably good, $\sigma \sim 5.4 \times 10^{-3}$ deg., and independent on the initial angle θ_0, as shown in Fig. 4 (a). For the vertical angle, ϕ, the blue triangles show the effect of the drift without any uncertainty on the time measurement $\sigma \sim 0.01$ deg. It is important to note that the rise of the ϕ angle difference for the most vertical angles is a consequence of the divergence of the sin ϕ function, which relates to the drift time. Consequently, the trend can be considered constant and fairly small. When including the electronic noise measured experimentally [20], in the time measurement, $\sigma_{TIME} = 26$ ns, the distribution gets wider and

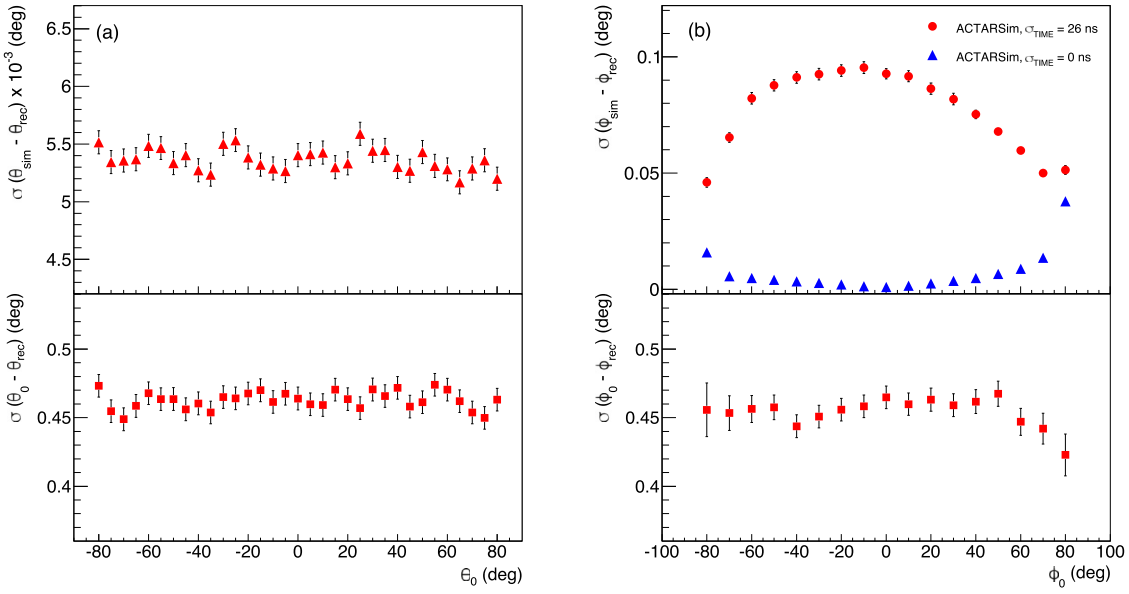

Fig. 4. (a) Reconstructed horizontal angle θ_{rec} resolution compared to the Geant4 simulated θ_{sim} (top) and to the initial particle angle $\theta_\circ$ (bottom).(b) Reconstructed vertical angle ϕ_{rec} with and without adding the pad time resolution, σ_{TIME}, compared to the Geant4 simulated ϕ_{sim} (top) and to the initial particle angle $\phi_\circ$ (bottom). σ_{TIME} is set to 26 ns (sigma), which corresponds to the experimental results obtained with the pulser [20].

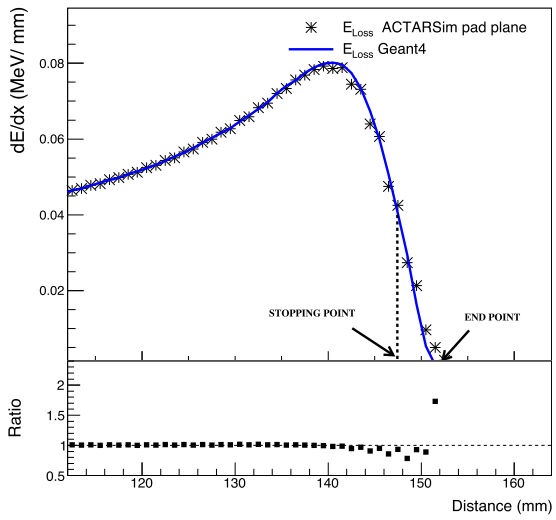

Fig. 5. (Color online.) Top-Average alpha energy loss profile, (E_{Loss}), obtained with ACTARSim from the Geant4 interacting points (blue solid line) and after digitization (black points). The figure shows the end point and the stopping point (see text for definition). Bottom-Ratio between the energy loss before and after digitization. (The ratio of the last point increases up to a factor $\simeq 8$, we have therefore chosen not to show it in the figure for the presentation purpose).

increases up to 0.1 deg. The resolution is worse for the angles parallel to the pad plane ($\phi_0 = 0$) and improves as the vertical angle increases or decreases. The shape is due to the effective amount of interaction points generated by the simulation per pad. While the number of interaction points simulated by Geant4 along the trajectory is the same for both angles, assuming the same energy of the alpha particle, the number of activated pads decreases as the slope of the track deviates from $\phi = 0$. Therefore the ratio of simulated points per pad for ($\phi_0 \neq 0$) has lower statistical fluctuations than for ($\phi_0 = 0$). This result is in agreement with the angular resolution of 0.06 deg (FWHM) obtained with a laser. [10]

The bottom panels of Figs. 4 (a) and (b) display the total uncertainty of the reconstruction procedure including straggling effects. Overall the resolution is found to be very good, of the order of 0.45 deg. in both cases. It is important to note that the angular resolution is mainly dominated by the straggling effects as the impact of the reconstruction procedure is negligible for both angles. In general, the quality of the reconstruction procedure is shown to be below 0.5 deg. Since the angular straggling within the gas depends on the experimental conditions, it will vary, according to the straggling formula, with the sort of particle and the type of gas. Nevertheless, the value of < 0.5 deg. obtained here represents a good estimation of the limiting factor induced by the straggling on the angular resolution for alpha particles in iC_4H_{10}. As a matter of fact, the study carried out here reveals that, in this configuration, it is the interaction of the particles with matter that dominates the angular resolution.

Regarding the energy loss profile (see Fig. 5), we have compared the average profile obtained from the energy loss of all the interaction points in Geant4 to the reconstructed average profile after digitization. The difference between them is visible only at the end of the track. The spread of the charge over the pads when the detector response is accounted for is the responsible for this effect. The reconstruction of the energy loss is in very good agreement with the one obtained directly from the interacting points in Geant4, apart from the last two points where the statistical uncertainties are really significant.

5. Comparison with experimental results

Alpha energy loss validations were carried out with an alpha source to determine the prediction power of models in Geant4 using the reconstruction procedures previously described. All data presented here were taken with a triple-alpha source using the experimental set-up described in Section 3. The tracks were further restricted to ± 10 deg. using the reconstructed ϕ; no cuts had to be applied on the θ angle. During the experiment the source was placed 36 mm away from the pad plane inside the gas volume, consequently the alpha particles lose energy before reaching the detection region. The simulations shown here include all the modifications of the set-up encountered during the data taking.

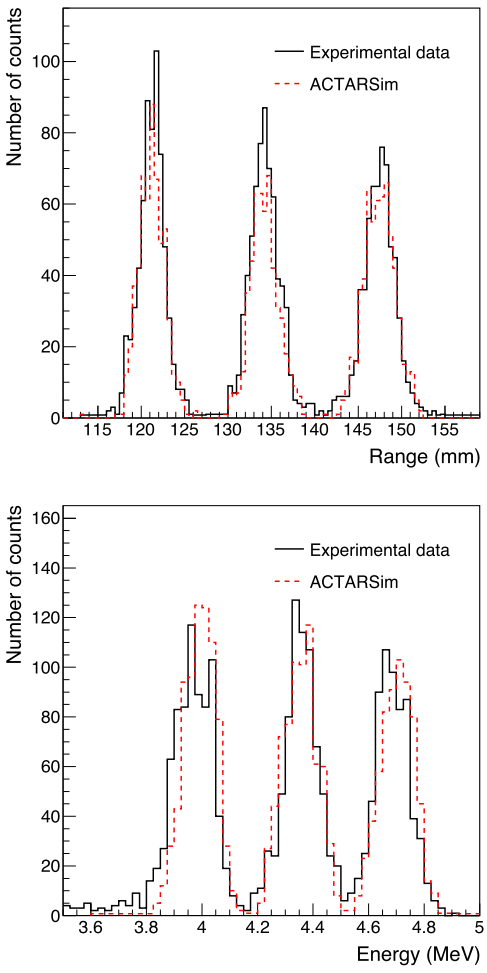

Fig. 6. (a) Simulated range (red dashed line) compared to experimental data (black solid line). (b) Calibrated experimental pad plane energy from alphas (black solid line) and simulated energy (red dashed line).

5.1. Range calculation

The range of the alpha particle at a given energy was calculated from the energy loss profile using the analysis techniques described in Section 4.2. In order to avoid statistical fluctuations in the determination of the range of the alphas inside the gas, we have used the particle "Stopping Point" which is defined as the position after the Bragg peak where the energy loss is equal to one half of the maximum (see Fig. 5).

A comparison between the range calculated from the simulation and experimental data is plotted in Fig. 6(a). The spectrum shows 3 peaks corresponding to the different energies of the alpha particles. The mean values obtained from these peaks are 121.2(1) mm, 134.1(1) mm and 147.5(1) mm for 5.15 MeV, 5.48 MeV and 5.8 MeV, respectively. The range standard deviations due to the particle straggling are 1.45(7) mm, 1.62(8) mm and 1.75(8) mm. These values correspond to an energy resolution of 1.7(1)%, 1.4(1)%, and 1.7(1)%, respectively. From Table 1, we can see that these values are in good agreement with ACTARSim and with TRIM [27] for both range and straggling.

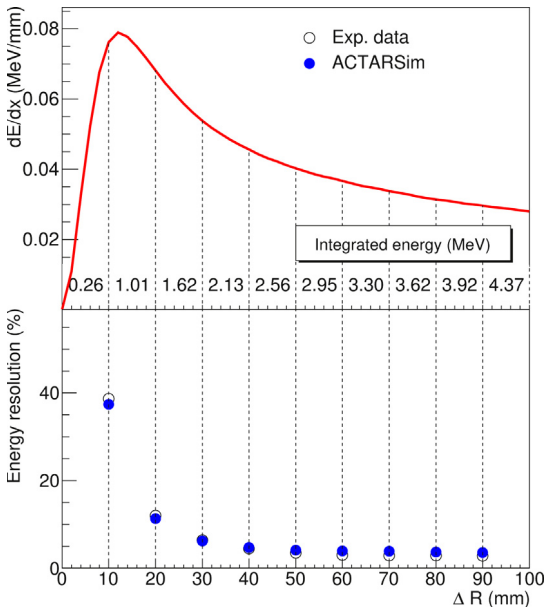

Fig. 7. Bragg peak (top) and energy resolution (bottom) as a function of the distance ΔR from the end point.

Table 1
Characteristic energies of the 3α source, E_α, experimental range, R^{exp}, and straggling, σ^{exp}, simulated range with ACTARSim R^{sim}, and straggling, σ^{sim}, and with TRIM range, R^{TRIM}, and straggling, σ^{TRIM}, in iC_4H_{10} at 105.6 mbar.

Radioactive source	E_α (MeV)	R^{exp} (mm)	σ^{exp} (mm)	R^{sim} (mm)	σ^{sim} (mm)	R^{TRIM} (mm)	σ^{TRIM} (mm)
^{239}Pu	5.15	121.2(1)	1.41(5)	121.2(1)	1.38(4)	121	1.34
^{241}Am	5.48	134.1(1)	1.61(6)	134.2(1)	1.60(7)	134	1.48
^{244}Cm	5.8	147.5(1)	1.65(7)	147.5(1)	1.79(6)	147	1.69

5.2. Energy resolution

For the study of the energy resolution, only the widths of the three alpha peaks are important, therefore the total charge deposited in the pads has been calibrated using the simulations.

5.3. Energy loss profile

The energy spectrum shown in Fig. 6(b) was obtained from the total charge collected on the pad plane. The three peaks corresponding to the different alphas' energies are well defined and have experimental resolutions of 4.1(6)%, 3.2(5)% and 3.0(4)% (FWHM) with increasing energy. These are in good agreement with ACTARSim resolutions which are 3.4(2)%, 3.5(2)% and 3.0(1)% respectively. It is important to note that the range measurement gives almost a factor two better energy resolution and provides a much more precise determination of the energy.

Since the Bragg peak shape is the same for any alpha energy in the same conditions (same θ and ϕ), one can study the energy resolution as a function of the distance ΔR from the end point. This is equivalent to studying the energy resolution as a function of the alpha energy. For this purpose we have integrated the energy-loss profile for different values of ΔR. Fig. 7 shows the evolution of energy resolution with ΔR. We can see that for ΔR =10 mm the resolution is poor because of the statistical fluctuations associated with the tiny integrated portion of the energy loss, dE/dx, deposited in the gas. For increasing ΔR, the area of the dE/dx signal gets larger, reducing the effect of the statistical fluctuations. Above ΔR = 40 mm the energy resolution remains almost constant around 4% (FWHM). More importantly, the trend of the energy resolution is well reproduced by the simulation, as Fig. 7 shows. The results obtained here are adapted to active targets with an amplification stage and with no magnetic field. The extended performance of ACTARSim to other systems such as pure ionization chambers, active targets with magnetic fields, will have to be further demonstrated.

5.4. Energy loss profile

For each alpha particle, the longitudinal and transverse profiles were obtained on an event-by-event basis at three different vertical angles (0° and ± 10°). Both profiles, longitudinal and transverse, are calculated from the three-dimensional energy-loss curve of the alpha particle within the gas. While the longitudinal profile is obtained from the Bragg curve along the particle direction, the transverse profile is the projection on a plane perpendicular to the track direction. The plots on the right-hand side of Fig. 8 show the width of the transverse profile as a function of distance. For each angle, the resulting average profile, calculated as discussed in Section 4.2, was used to compare with the simulations. The simulated longitudinal and transverse profiles are compared to the experimental results in Fig. 8, where the height and longitudinal shift of the simulations have been adjusted to align the shapes. The results of the simulations for the energy-loss profiles (dE/dx) along the track, shown in the left panel of Fig. 8, display a narrower shape compared to the experimental data. The relative deviation, defined as the difference between the experiment and the simulation divided by the experimental value for each bin, is well below 5% throughout the full track and reaches 20% just for the last point of the track, where other effects dominate. The origin of this slight disagreement in shape might come from some unaccounted features in the energy loss calculations of alphas by Geant4.

The transverse profile at $\phi = 0$ deg. shows a very good agreement with the experimental data. It is important to note that the value of the transverse diffusion factor D_T, as determined using MAGBOLTZ, had to be reduced by 17% in order to match the data. This is due to second order effects produced by the difficulty to adjust the thresholds simultaneously to different type of parameters. The adopted value is $D_T = 20.70 \times 10^{-2}$ mm^2/μs. For vertical angles different from zero, the results differ whether the particles have been emitted towards the top or bottom of the pad plane. While for upward vertical angles, $\phi = 10^o$, the results from the simulations are compatible with the data, for downward vertical angles, $\phi = -10^o$, the dispersion is underestimated by the simulations. Despite the impact of this effect being small, of the order of 0.02 mm compared to the pad size of 2 mm, it is a systematic effect that is not properly accounted for in the simulations.

6. Conclusion

This paper shows the performance of the ACTARSim software for alpha particles. First, we have studied the quality of the reconstruction method. In general, the attained resolution is of the order of 0.5 deg. for the horizontal and vertical angles, well within the standard resolution for modern active targets. It is interesting to note that the quoted uncertainty on the angular reconstruction is mainly dominated by straggling effects as the effects of the reconstruction are negligible. Interestingly, this poses a limit in the performance of the detector induced by the straggling itself. The reconstructed average profile shows a good agreement with GEANT4 calculations.

Second, a validation of the ACTARSim software was performed using experimental data of alpha particles in iC_4H_{10} measured with the ACTAR TPC demonstrator. Range and straggling simulations show a good agreement with experimental data. Energy resolution was found to be approximately 1.5% FWHM from the range and 3.5% FWHM from the collected charge in both simulation and experimental data.

Longitudinal and transversal profiles have been compared to the ACTARSim simulations. Longitudinal profiles are in rather good agreement and they do not depend on the vertical angle. Transversal profiles are shown to have some unaccounted effects on the description of

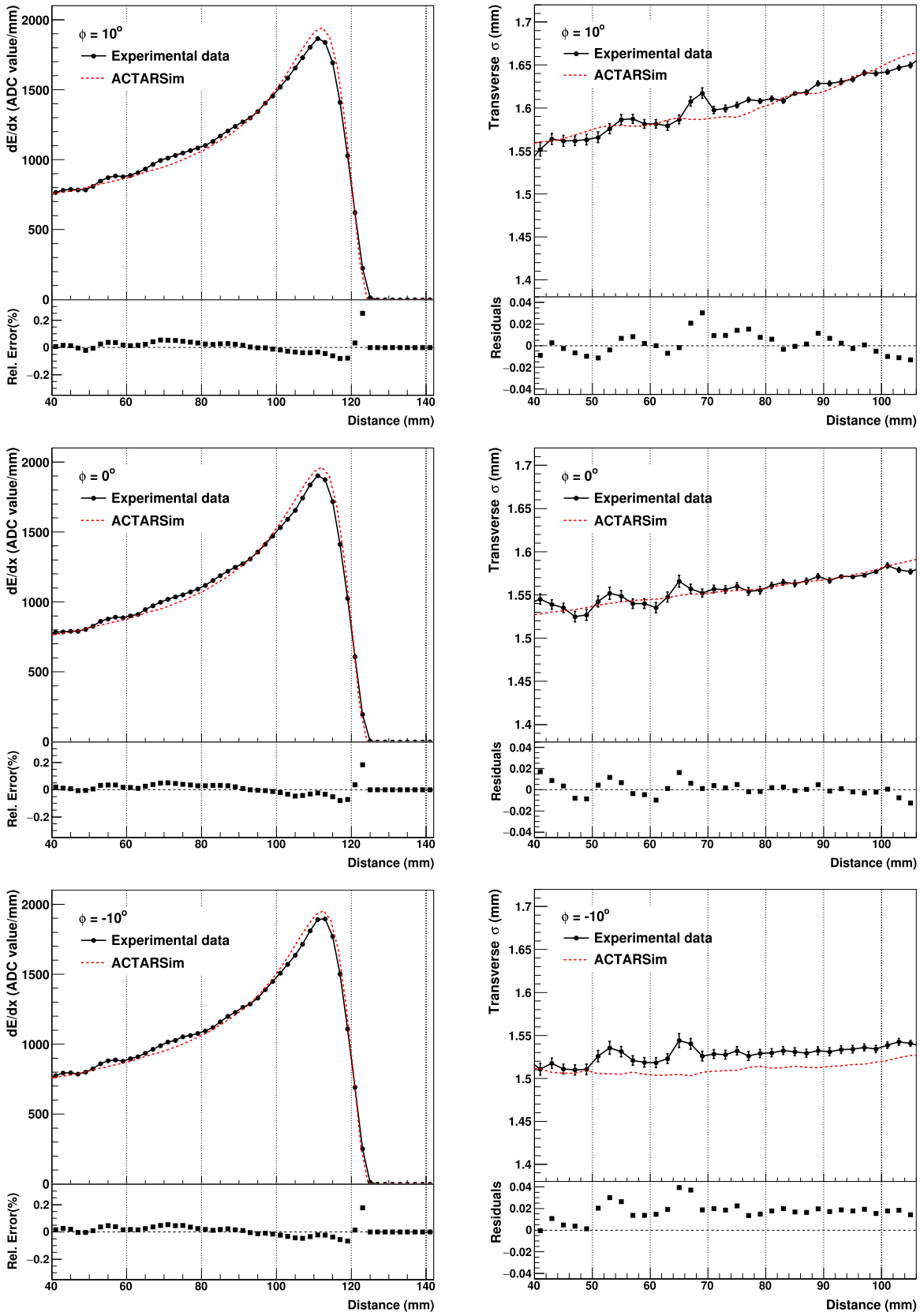

Fig. 8. Longitudinal (left) and transverse (right) alpha energy deposit profiles compared to simulations (dashed red lines) for horizontal angle $\theta = 0°$ and vertical angle $\phi = 10°$ (top), 0° (middle) and −10° (bottom). Bottom panel of the longitudinal profiles show the relative error (see text for description), and the ones of the lateral profiles show the residuals, σ_T^{exp}- σ_T^{sim}.

the negative vertical angles, although the impact of this difference has been proven to be small enough. In general, adjustment of the experimental profiles with simulated ones at different vertical angles are in good agreement. This indicates that light particle interactions inside the detector are well reproduced by Geant4. Further validation of ACTARSim with heavier ions is planned.

Acknowledgments

The authors acknowledge the support provided by the technical staff of GANIL. This work is supported by the Xunta de Galicia (Spain) grant Emerxentes 2013-PG015. B.F.D. and M.C.F acknowledge financial support from the Ramón y Cajal programme RYC-2010-06484 and RYC-2012-11585 and from the Spanish MINECO grant No. FPA2015-71690-P. The research leading to these results has received funding from the European Research Council, European Union under the European Unions Seventh Framework Program (FP7/2007–2013)/ERC grant agreements no 335593 and 617156.

References

[1] G.D. Alkhazov, et al., Phys. Rev. Lett. 78 (1997) 2313.
[2] P. Egelhof, Prog. Part. Nucl. Phys. 46 (2001) 307.
[3] B. Blank, et al., Nucl. Instrum. Methods A 613 (2010) 65.
[4] J. Giovinazzo, et al., Phys. Rev. Lett. 99 (2007) 102501.
[5] I. Tanihata, et al., Phys. Rev. Lett. 100 (2008) 192502.
[6] T. Roger, et al., Phys. Rev. C 79 (2009) 031603(R).
[7] M. Caamao, et al., Phys. Rev. Lett. 99 (2007) 062502.
[8] C. Demonchy, et al., Nucl. Instrum. Methods A 573 (2007) 145.
[9] https://www.blogs.uni-mainz.de/fb08-mami-experiments/files/2017/11/ep_-proposal.pdf.
[10] T. Roger, et al., Nucl. Instrum. Methods A 895 (2018) 126–134.
[11] D. Suzuki, et al., Nucl. Instrum. Methods A 691 (2012) 39–54.
[12] R. Shane, et al., Nucl. Instrum. Methods A 784 (2015) 513.
[13] https://fair-center.eu/fileadmin/fair/publications_exp/TDR_R3B_ACTAF_public.pdf.
[14] H. Alvarez-Pol, et al., NIM (2019) in preparation, https://github.com/ActarSimGroup/Actarsim.
[15] S. Agostineli, et al., Nucl. Instrum. Methods A 506 (2003) 250.
[16] R. Brun, F. Rademakers, Nucl. Instrum. Methods A 389 (1997) 81–86, See also http://root.cern.ch/.
[17] S. Biagi, Nucl. Instrum. Methods A 421 (1999) 234.
[18] http://garfield.web.cern.ch/garfield/.
[19] http://garfieldpp.web.cern.ch/garfieldpp/.
[20] J. Pancin, et al., Nucl. Instrum. Methods A 735 (2014) 532–540.
[21] T. Roger, et al., Nucl. Instrum. Methods A 638 (2011) 134.
[22] Y. Giomataris, et al., Nucl. Instrum. Methods A 376 (1996) 29–35.
[23] Y. Giomataris, et al., Nucl. Instrum. Methods A 560 (2006) 405–408.
[24] E.C. Pollacco, et al., Nucl. Instrum. Methods A 887 (2018) 81.
[25] W.R. Leo, Techniques for Nuclear and Particle Physics Experiments, second ed., Springer-Verlag, 1994.
[26] R. Bellazzini, et al., Nucl. Instrum. Methods A 581 (2007) 246.
[27] J.Z. Ziegler, et al., Nucl. Instrum. Methods B 268 (2010) 1818.